The Second Generation HRRT – a Multi-Centre Scanner Performance Investigation

Vesna Sossi, Hugo W.A.M. de Jong, W. Craig Barker, Peter Bloomfield, Ziad Burbar, Marie-Laure Camborde, Claude Comtat, Lars A. Eriksson, Sylvain Houle, David Keator, Christof Knöß, Roman Krais, Adriaan A. Lammertsma, Arman Rahmim, Mérence Sibomana, Mika Teräs, Christopher J. Thompson, Régine Trébossen, John Votaw, Matthew Walker, Klaus Wienhard and Dean F. Wong

***Abstract*— The high resolution research tomograph (HRRT) is one of the most complex existing Positron Emission Tomographs: it is the only human size scanner capable of decoding the depth of the γ-ray interaction in the crystal, using a lutetium LSO/LYSO phoswitch detector arrangement. In this study we determined basic scanner hardware characteristics, such as scanner data acquisition stability, and their variability across eleven centres. In addition a subset of the NEMA NU-2001 standards measurements was performed. We found *(i)* significant variability in the DOI decoding results between centres, *(ii)* a trend toward an increasing number of detected true coincident events as a function of elapsed time from scanner calibration likely due to a shifting energy spectrum, *(iii)* a count-rate dependent layer identification, *(iv)* scatter fraction ranging from $\sim$ 42% to 54% where the variability was partly related to the shifting of the energy spectrum, *(v)* sensitivity ranging from $\sim$ 5.5% to 6.5% across centres, *(vi)* resolution of $\sim$ (2.5mm)^3, fairly consistent across centres, *(vii)* image quality which is very comparable to other scanners.**

***Index Terms*— PET, Positron Emission Tomography, ECAT HRRT, high resolution research tomograph, performance study, stability, depth of interaction, scatter fraction, sensitivity, resolution.**

V. Sossi is with the Physics and Astronomy Department, University of British Columbia, Vancouver, Canada

H.W.A.M. de Jong and A.A. Lammertsma are with the Department of Nuclear Medicine & PET Research, VU University Medical Centre, Amsterdam, The Netherlands, EU

W.C. Barker is with the PET Department, NIH Clinical Centre, National Institute of Health, Bethesda, Maryland, USA

P. Bloomfield and S. Houle are with the Centre for Addiction and Mental Health, Toronto, Canada

Z. Bubar and M. Sibomana are with CTI PET Systems (Siemens Medical Solutions), Knoxville, Tennessee, USA

M.-L. Camborde is with the Pacific Parkinson's Research Centre, University of British Colombia, Vancouver, Canada

C. Comtat and R. Trébossen are with the Frédéric Joliot Hospital Facility, CEA/DSV, Orsay, France, EU

L.A. Eriksson and M. Walker with the Wolfson Molecular Imaging Centre, The University of Manchester, Manchester, Great Britain, EU

D. Keator is with the Psychiatry & Human Behaviour Department, University of California, Irvine, California, USA

C. Knöß and K. Wienhard are with the Max-Planck-Insitute for Neurological Research, Cologne, Germany, EU

R. Krais and M. Teräs are with Turku PET Centre, Turku, Finland, EU

A. Rahmim and D.F. Wong are with the Radiology Department, The Johns Hopkins University School of Medicine, Baltimore, Maryland, USA

C.J. Thompson is with the Montreal Neurological Institute, McGill University, Montreal, Canada

J. Votaw is with the Radiology and Physics Department, Emory University, Atlanta, Georgia, USA

This is the conference record of poster M07-269, Med.Imag.Conf Oct. 2005, Puerto Rico

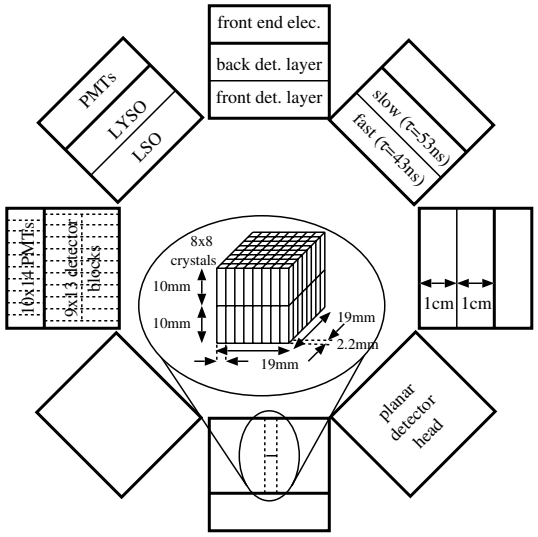

Fig. 1. Detector arrangement in the ECAT HRRT. PMT quadrant sharing detector design realised in eight planar detector heads, containing front end readout electronics, a "slow" (LYSO) and "fast" (LSO) detector layer

I. Introduction

THE high resolution research tomograph (ECAT HRRT - CTI PET Systems - see fig. 1) is one of the most complex existing Positron Emission Tomographs (PET) [1] [2] [3]. It is the only human size scanner with a resolution of about 2.5 mm (axially and transaxially) and a phoswitch detector making use of crystals with different decay times for depth of interaction (DOI) determination by pulse shape discrimination [4]. The two 1 cm thick detector layers are made of cerium-doped lutetium oxyorthosilicate (LSO, Lu_2SiO_5:Ce) and cerium-doped lutetium-yttrium oxyorthosilicate (LYSO, $Lu_{0.6}Y_{1.4}SiO_5$:Ce, i.e. 70% YSO and 30% LSO) with decay times of 43-44 ns and 53 ns [5] [3], respectively. The lutetium in the crystal contains 2.6% ^{176}Lu, which is a β-emitter itself. The photomultiplier tube (PMT) quadrant sharing detector design requires the overall 119,808 2.2x2.2x10 mm^3 detectors of the 3D only scanner to be assembled in planar detector heads. The field of view (FOV) of the dedicated brain scanner measures 25 cm in axial and 35 cm in transaxial direction, the resulting slice thickness is 1.22 mm. Transmissions scans are performed with a ^{137}Cs point source (662 keV γ-emitter, $T_{1/2}$=30.2 a). A

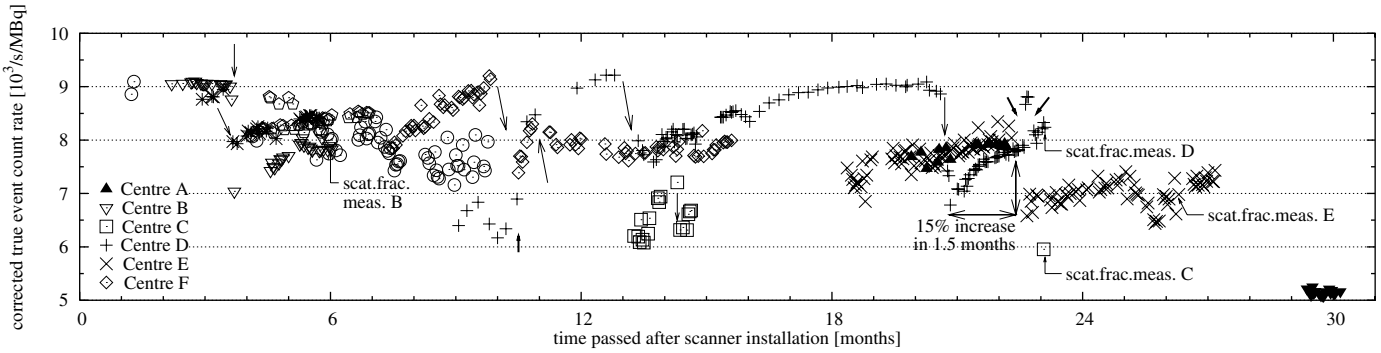

Fig. 2. Dead-time corrected true event count-rate normalised to radioactivity in the phantom - a measure of the scanner sensitivity. The data were obtained in eleven different centres (each symbol always corresponds to the same centre). The x-axis shows the time after scanner installation at which the experiments were performed so as to take into account the age of the electronic and PMTs. Discontinuous changes in sensitivity related to a set-up are marked with long arrows, those not related to any set-up with short arrows.

carefully done full detector set-up is very complex, requires a lot of user interaction and takes about one week.

The first prototype HRRT was installed in 1999 [3], a second, single layer prototype in 2002. Between June 2002 and spring 2005, twelve tomographs of the so called second generation were installed in PET centres across North America and Europe.

The aim of this multi-centre study is to determine basic scanner performance parameters such as DOI determination and detection sensitivity, to describe their stability over time and to provide an estimate of their variability between scanners. Some of the eleven participating centres have also measured scanner spatial resolution, scatter fraction, count-rate performance and performed an image quality study to obtain an overall performance assessment of this scanner that closely follows the NEMA NU 2-2001 and NU 2-1994 guidelines.

II. Hardware Performance

A. Stability of Sensitivity in Emission Mode

1) Methods: A 5 min long scan of a uniformity phantom (cylindrical 20 cm diameter, 27 cm long, activity range 5-90 MBq ^{68}Ge, energy window 400-650 keV) was performed for a minimum of 25 days. Dead-time corrected true event rate normalised to phantom activity is a measure for the scanner sensitivity and was considered the main figure of merit in this experiment. In order to gain some understanding of the observed true rates behaviour a series of 30 s scans with different 10 keV wide energy windows (200-210 keV, 210-220 keV, ...) was performed on one scanner with a 7 MBq ^{68}Ge line source in the centre of the FOV. The average block singles were plotted versus the position of the energy window to get a kind of effective, gantry representative "spectrum" of 511 keV photons.

2) Results and Discussion: The results are presented in fig. 2. There is up to 40% variation in the corrected true event rate between centres. Most scanners show an increasing true event rate as a function of elapsed time. Drifts of up to 10% in three weeks were seen. Changes of the true rate of up to 15% were observed after detector set-up (marked with long arrows).

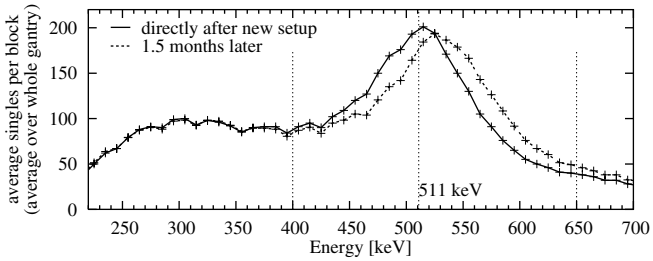

Fig. 3. Effective 511 keV "whole-gantry-spectrum" of a ^{68}Ge line source, measured in centre D once directly after a detector set-up and once 1.5 month later. In the corresponding time the corrected true event count-rate in a 400-650 keV energy window increased by 15% (marked in fig. 2)

In addition a few discontinuous changes not related to detector set-up were observed (short arrows). The data indicate that the drift is neither directly correlated to the age of the PMTs/gantry nor to the level of radioactivity in the phantom.

The "spectrum" acquired once immediately and once 1.5 months after a detector set-up (see fig. 3, acquisition times are marked in fig. 2) shows an unexpected behaviour. It has been reported earlier [6] that the gain of aging Philips XP1911 PMTs used in the HRRT [3] is decreasing. However, for the HRRT a drift of the "spectrum" toward higher energy channels was observed, which is deemed to explaining the corresponding 15% increase in sensitivity as more scatter events are getting included. At present its origin is not well understood.

B. Depth of Interaction (DOI) Determination

1) Methods: The phantom measurements described in II-A.1 were also used to investigate the relative sensitivity of the back detector layer. The counts (prompts + delayed) were assigned to the back (L_b) or front (L_f) layer (each coincidence makes two counts). The ratio of counts in the back layer $\frac{L_b}{L_f+L_b}$ was determined for each detector head separately. Results are presented as mean across the eight detector heads and corresponding standard deviation. In addition, a Monte-Carlo simulation of the experimental conditions using PETSIM was performed to obtain a theoretical value for this ratio [7] [8]. The

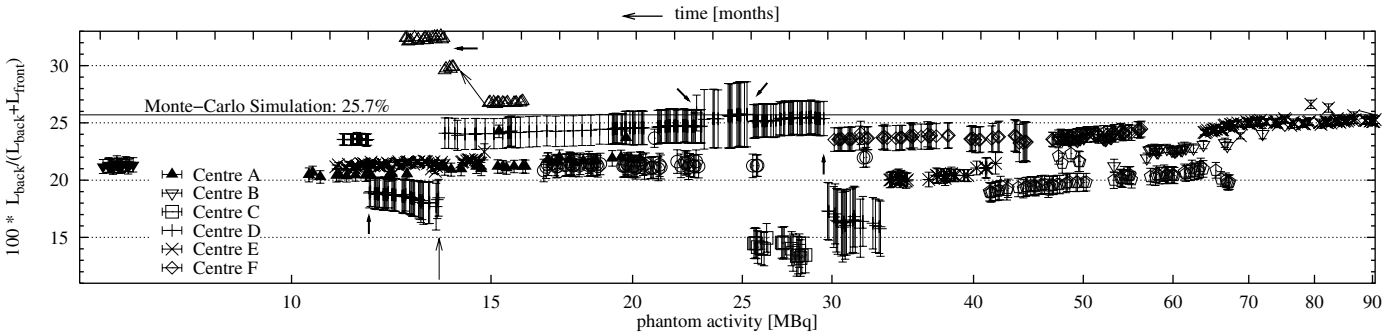

Fig. 4. Ratio of counts in the back detector layer $\frac{L_b}{L_f+L_b} \cdot 100$ obtained in eleven different centres (each symbol always corresponds to the same centre). The logarithmic x-axis shows the radioactivity present in the ^{68}Ge uniformity phantom at the time of the scan. Since the phantom is decaying the x-axis corresponds to an inverse time axis. Discontinuous changes related to a set-up are marked with long arrows, those not related to any set-up with short arrows.

following settings were used for the simulation: 20 cm diameter, 31 cm long water filled cylinder centrally placed in the HRRT scanner; linear attenuation coefficients of 0.785 cm^{-1} (LSO) and 0.493 cm^{-1} (LYSO); 20% FWHM at 511 keV; no random events; no scattered events; only those γ-events were considered which deposit energy in only one detector layer.

2) Results and Discussion: The results are presented in fig. 4. The Monte-Carlo simulation predicts a ratio of 25.7%. While most detector heads show ratios in the expected range of 20-25% there is still a significant variability between heads in different centres (from 10.1% to 34.9%). This, the large variability in the magnitude of the standard deviation amongst heads and discontinuous changes related to set-up modifications (marked with long arrows) and changes not related to set-up modifications (marked with short arrows) indicate problems with the robustness of the detector set-up. Data from most centres show a decrease of the ratio as a function of decreasing phantom activity. This can be attributed to event DOI mis-identification at higher count rates [9].

C. Stability of Sensitivity in Transmission Mode with ^{137}Cs

1) Methods: Standardised transmission blank scans (energy window 550-800 keV) with the approx. 1.1 GBq ^{137}Cs point transmission source were performed for at least 25 days. The total number of events in those scans were normalised to the number of events in the first scan of the series to account for differences in transmission source strength and geometry.

2) Results and Discussion: The results are presented in fig. 5. Several centres show a small drift toward higher or lower count-rates while others show a very stable count-rate. A clear link between the drift in the corrected trues rate (fig. 2) and the drifting prompts rate in the ^{137}Cs scan could not be found.

III. Global Characteristics

A. Spatial Resolution

1) Methods: Resolution was measured according to the NEMA NU 2-2001 method. Data were reconstructed iteratively using 3D Ordinary Poisson OSEM (span 3 and 9, 10 iterations, 16 subsets).

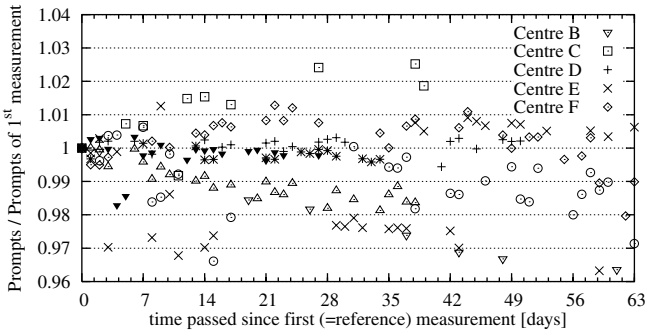

Fig. 5. Number of events in a ^{137}Cs blank scan recorded as a function of time normalised to the value obtained at the beginning of the experiment

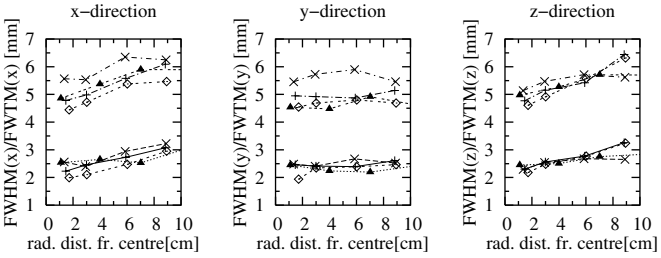

Fig. 6. NEMA NU 2-2001 resolution in Centres A, D, E, F

2) Results and Discussion: The results are presented in fig. 6. Very consistent results are obtained for the scanners, and a very good resolution uniformity (due to DOI) is observed.

B. Absolute Sensitivity

1) Methods: Sensitivity was measured using the method of sleeves [10] adopted by NEMA NU 2-2001.

2) Results and Discussion: The results are presented in table I. The sensitivity measured in the centres seems to be clustered around two values; One group is in the mid five percent range and the other in the mid six percent range.

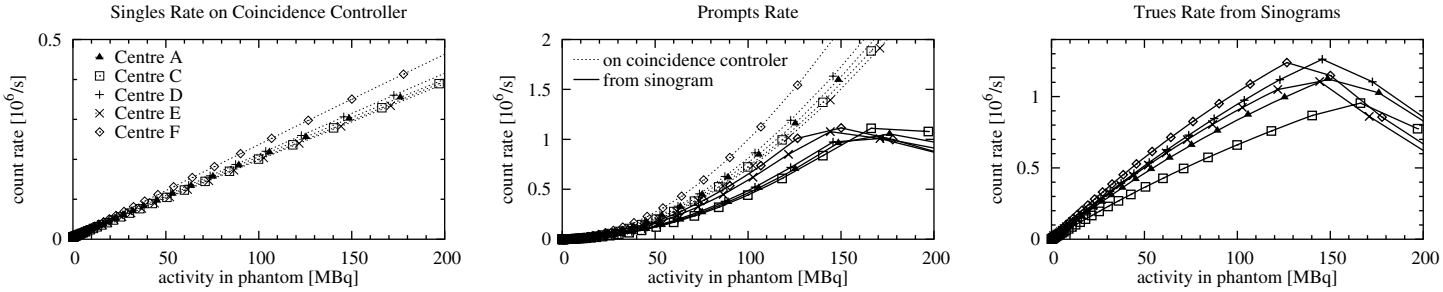

Fig. 7. Curves of the count-rate study. Each symbol always corresponds to the same centre.

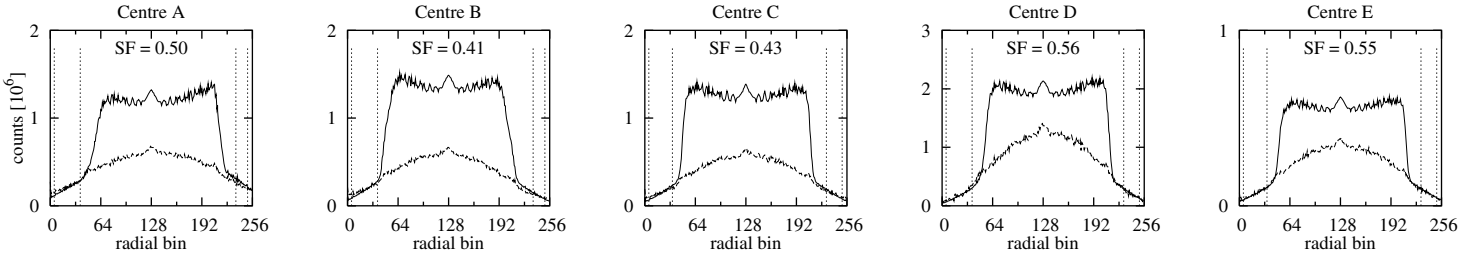

Fig. 8. Radial profiles, summed over the angular directions and the central 100 slices, are shown for the scattered + unscattered and the scattered only coincidences. The vertical lines show the limits used to adjust both profiles on the tails of the distributions.

Centre	A	B	C	D	E	F
Sensitivity	5.6%	5.3%	-	6.5%	6.5%	5.6%
Scatter Fraction	50	41	43	56	55	-

TABLE I
Abs. point source sensitivity (centre FOV) and scatter fraction

	Range	Range %
total vol. sensitivity at $\ll$1kBq/ml	39.8-74.4 kcps/kBq/ml	61%
max. Singles rate on Coinc. Contr.	22-27 Mcps	20%
max. Prompts rate on Coinc. Contr.	1.9-2.6 Mcps	33%
max. Prompts rate in sinograms	1.4-2.0 Mcps	39%
max. Trues rate in sinograms	0.76-1.18 Mcps	46%
Error in linearity (dead-time correction)	0.6-5.3%	

TABLE II
Results of count-rate study. The sensitivity includes scatter. The rates are measured with 20 kBq/ml in FOV.

C. Count-Rate

1) Methods: This experiment was performed with a cylindrical 20 cm diameter, 20 cm long phantom centred axially and radially, filled with an initial activity of approximately 300 MBq of ^{11}C. List mode data were acquired for 200 min ($\sim$ 10 half-lives) and binned into 5 min intervals.

2) Results and Discussion: The results are presented in fig. 7 and table II. The volume sensitivity varies widely between centres. The centre-to-centre variation is smallest when comparing singles rate as found on the coincidence controller (beginning of the acquisition process) and largest when comparing the trues rate as found in the acquired sinograms (end of the acquisition process). The dead-time correction varies between excellent (0.6% error at 20 kBq/cc) and poor (5.6% error at 20 kBq/cc).

D. Scatter Fraction

1) Methods: Scatter fraction was determined by off-setting the cylinder axially and evaluating the functional form describing the shape of the scattered coincidences profile just outside the phantom; this functional form was then fitted to the tails of the scattered plus unscattered coincidences profiles in the low count-rate scan (see III-C) to determine the scatter fraction.

2) Results and Discussion: A representative set of plots used to obtain the scatter fraction and the corresponding SF values is shown in fig. 8. The quality of the tails fit is not very satisfactory for centres A and B, and their respective scatter fraction is uncertain. There is a variability in the scatter fraction between centres as can be seen from table I. This variability has been found to be partly related to the variability in the number of acquired true events (fig. 2), which, in turn is related to the shifting of the energy spectra. The corrected trues event count-rates measured in centres B, C, D and E at the time of the scatter fraction measurements are marked with arrows in fig. 2.

Monte-Carlo simulation studies investigating the relative contribution of scattered and true events to different regions of the energy spectrum (fig. 9) indicate that an increase in gain of the energy spectrum would greatly enhance the contribution of scattered events, while hardly affecting the number of unscattered events.

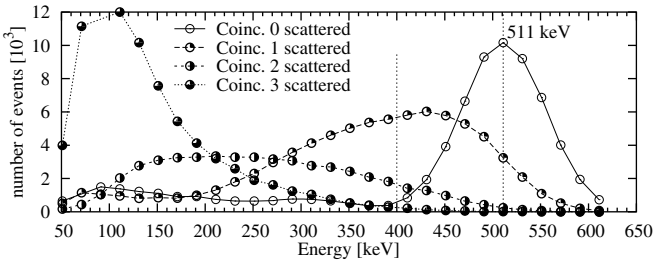

Fig. 9. Monte Carlo simulated spectrum. Relative contribution of true (threshold 400 keV), single, double and triple scatter to the energy spectrum.

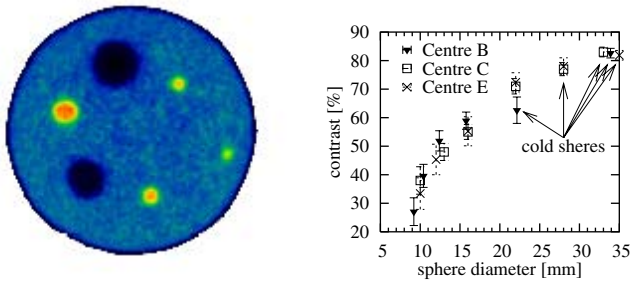

Fig. 10. Left: Image of the Jaszczak phantom scanned for image quality measurement. It contains 6 fillable spheres ranging from 10 to 35 mm diameter. Right: Resulting contrasts and standard deviations in three centres.

E. Image Quality Measurement

1) Methods: Three centres measured the Jaszczak phantom with six spheres (approximate ID: 10, 12, 16, 22, 28 and 35 mm - slightly different size spheres were used). The phantom was filled with an initial activity of approximately 37 MBq; the four smaller spheres provided a contrast of $\sim$ 5:1 (hot spheres), while the two bigger spheres were filled with water (cold spheres). Data were acquired for 180 min and in order to estimate variance in the determined contrast figures - binned into interleaved five minutes frames (each five minutes of data were divided into 36 segments each segment contributed to a different final frame) so as to create 36 statistically independent replicas. Regions of interest (ROIs) following the inside diameter of the spheres were placed on each sphere and sets of 60 ROIs with diameter corresponding to those of the each sphere ROI were placed on the background region. The data were reconstructed iteratively in 3D Ordinary Poisson OSEM span 3, 16 subsets and 6 iterations with 2mm post-smoothing. Figures of merit used were:

(i) Percent contrast $Q_{H,j}$ for each hot sphere $j = \frac{C_{Hj}/C_{Bj}-1}{a_H/a_B-1} \cdot 100\%$, where $C_{H,j}$ is the average counts in the ROI for sphere j , $C_{B,j}$ is the average of the background ROI counts for sphere j, a_H is the activity concentration in the hot spheres and a_B is the activity concentration in the background.

(ii) Percent contrast $Q_{C,j}$ for each cold sphere $j = \frac{1-C_{Cj}}{C_{Bj}} \cdot 100\%$ with similar parameter meaning.

2) Results and Discussion: An image of the image quality phantom scanned with four hot spheres and two cold spheres and the resulting contrast is shown in fig. 10. The results are very consistent for the two centres and are also consistent with the data published for other scanners [11].

IV. Conclusion

This study describes – as far as know – the first large scale multi-centre comparison of a PET scanner characteristics. HRRT scanner performance and stability were monitored in eleven participating research centres. The scanner resolution was found to be consistently $\sim (2.5\text{mm})^3$ and relatively uniform across the entire FOV in spite of an observed count-rate dependent DOI layer identification, demonstrating the superior resolution properties of this scanner. Significant variability amongst centres was observed for several measured parameters: DOI decoding, scatter fraction (ranging from $\sim 42\%$ to $\sim 54\%$) and absolute sensitivity (ranging from 5.5% to 6.5%). Such variation was at least partially attributed to a shifting energy spectrum that greatly changes the fraction of the scattered events in the allowed energy window. Such shift is likely related to a drift in the number of detected true events (up to 10% in three weeks) that was observed in the majority of the centres. In most cases discontinuities in detection sensitivity were observed after the performance of a detector set-up procedure. These results illustrate the complexity of the scanner hardware and the strong dependence of scanner performance on the detector set-up. A frequent and accurate, ideally automated, calibration procedure is therefore necessary to minimise variations in scanner performance and potential operator-dependency.

References

[1] L. Eriksson et al., *The ECAT HRRT NEMA NEC evaluation of the HRRT system, the new high-resolution research tomograph*, IEEE Trans Nucl Sci 49:2085-2088, 2002

[2] K. Wienhard et al., *The ECAT HRRT: Performance and first clinical application of the new high resolution research tomograph*, IEEE Trans Nuc Sci, 49 (1):104-110, 2002

[3] C. Knöß, *Evaluation and Optimization of the High Resolution Research Tomograph (HRRT)*, ISBN 3-8322-3337-7

[4] Young et al., *FPGA based front-end electronics for a high resolution PET scanner*, IEEE Trans. Nuc. Sci. 47(4), 1676-1680, 2000

[5] Pepin et al., *Investigation of the properties of new scintillator LYSO and recent LSO scintillators for phoswich PET detecotrs*, IEEE Med. Imag. Conf. Rec., 2002

[6] Uribe et al., *Effect of Photomultiplier Gain-Drift and Radiation Exposure on 2D-Map Decoding of Detector Arrays Used in PET*, Nucl. Sci. Symp. Conf. Rec., 2001

[7] M.J. Berger et al., *XCOM program documentation and instructions*, National Institute of Science and Technology (NIST)

[8] C.J. Thompson et al., *PETSIM: Monte Carlo Simulation of all Sensitivity and Resolution Parameters of Positron Imaging Systems*, Phys. Med. Biol. 37:3 731-749, 1992

[9] W.C. Barker et al., *Randoms Estimation for List-mode Reconstruction of the ECAT HRRT*, IEEE Med. Imag. Conf. Rec, M9-187, 2004

[10] DL Bailey et al., *A method for measuring the absolute sensitivity of positron emission tomographic scanners*, Eur J Nucl Med. 18(6):374-9, 1991

[11] O. Mawlawi et al., *Performance characteristics of a newly developed PET/CT Scanner using NEMA standard in 2D and 3D modes*, J. Nucl. Med.45:1734-1742, 2004